Progress of Theoretical Physics, Vol. 92, No. 5, November 1994

Numerical Simulation of Viscous Flow by Smoothed Particle Hydrodynamics

Hidenori TAKEDA, Shoken M. MIYAMA* and Minoru SEKIYA**

Department of Aeronautical Engineering, Kyoto University, Kyoto 606-01
**National Astronomical Observatory, Mitaka 181*
***Department of Earth and Planetary Sciences, Kyushu University Fukuoka 812*

(Received July 19, 1994)

Smoothed particle hydrodynamics (SPH) is an effective numerical method to solve various problems, especially in astrophysics, but its applications have been limited to inviscid flows since it is considered not to yield ready solutions to fluid equations with second-order derivatives. Here we present a new SPH method that can be used to solve the Navier-Stokes equations for constant viscosity. The method is applied to two-dimensional Poiseuille flow, three-dimensional Hagen-Poiseuille flow and two-dimensional isothermal flows around a cylinder. In the former two cases, the temperature of fluid is assumed to be linearly dependent on a coordinate variable x along the flow direction. The numerical results agree well with analytic solutions, and we obtain nearly uniform density distributions and the expected parabolic and paraboloid velocity profiles. The density and velocity field in the latter case are compared with the results obtained using a finite difference method. Both methods give similar results for Reynolds number R_e=6, 10, 20, 30 and 55, and the differences in the total drag coefficients are about 2~4%. Our numerical simulations indicate that SPH is also an effective numerical method for calculation of viscous flows.

§ 1. Introduction

Smoothed particle hydrodynamics (SPH) has been used to describe three-dimensional flows both in astrophysical problems[1)~5)] (see Monaghan[6)] for references) and laboratory problems[7)~10)] and has several advantages over finite difference methods (FDMs): 1) it is a Lagrangian method, and the amount of artificial angular momentum transport is thus expected to be less than that of FDMs; 2) no hard calculations for generation or rezoning of grids are necessary, even for complicated mass distribution; 3) no special treatments are necessary for multi-component fluids[11)] (see Cameron & Benz[12)] for references on astrophysical problems and see a review of Stellingwerf[7)] on simulations of non-astrophysical problems). Recently, a new SPH scheme has been found[13)] that reproduces shock waves with accuracies comparable to those of FDMs.

Many problems concerning astrophysical phenomena where viscosity plays an important role are solved by numerical simulations; for example, flows in accretion disks,[14)] planetary formation processes in proto-solar nebulae[15),16)] and the interactions between traveling galaxies and intergalactic medium.[17)] Numerical simulations have been mainly two-dimensional in given gravitational fields and performed by FDMs.

Real phenomena, however, are usually three-dimensional, including gravitational effects (often self-gravity is important), and the flows related with them involve compressible fluids. It is thus important to develop a hydrodynamic code for three-dimensional viscous flows including gravitational interactions.

We, therefore, have searched for a way to solve the Navier-Stokes equations using SPH. If found, such a method will be very useful both in physics and astrophysics. Here we present a new SPH formalism for dynamical motion of a three-dimensional, compressible, viscous fluid. We give definite SPH expressions for the Navier-Stokes equations and for boundary conditions, and we evaluate the method through stringent tests for the case of non-gravitating systems.

In § 2, the new SPH formalism for the Navier-Stokes equations is given. The method is tested by application to two-dimensional Poiseuille flow, Hagen-Poiseuille flow and flows around a cylinder. The results of the test are presented in §§ 3 and 4 and summarized in § 5.

§ 2. SPH formalism for the Navier-Stokes equations

Our main purpose is to give the expression of second order derivatives of velocities, the viscous terms. The equations with second order derivatives are solved for thermal conduction problems[18] with a method combining SPH with a finite difference method. Elastic-plastic solids problems are solved by SPH[8)~10)] where time dependent equations for stress tensors are solved in addition to density, momentum and energy equations. These calculations include only first order derivatives of a kernel. In this paper, we show that the straightforward second order derivatives of a kernel can be ued to solve the Navier-Stokes equations.

The smoothed particle hydrodynamics method presented here is based on the Monte Carlo method, which provides reasonable estimates of multiple integrals with a few points. First, we define the smoothed value $\langle f(\boldsymbol{x})\rangle$ for physical quantity $f(\boldsymbol{x})$:

$$\langle f(\boldsymbol{x})\rangle=\int W(\boldsymbol{x}-\boldsymbol{x}')f(x')d\boldsymbol{x}', \tag{2·1}$$

where W is a kernel function which satisfies the condition (see for example Gingold & Monaghan[2)])

$$\int W(\boldsymbol{x}-\boldsymbol{x}')d\boldsymbol{x}'=1. \tag{2·2}$$

In the SPH method, all physical values are given by the above smoothed value.

For discrete distribution of particles, the integral in Eq. (2·1) is approximated by the sum

$$\langle f(\boldsymbol{x})\rangle=\sum_j m_j \frac{f(\boldsymbol{x}_j)}{\rho(\boldsymbol{x}_j)} W(\boldsymbol{x}-\boldsymbol{x}_j), \tag{2·3}$$

according to the Monte Carlo theory. The expressions for density ρ and velocity $\boldsymbol{v}$ are given by

$$\langle \rho(\boldsymbol{x})\rangle=\sum_j m_j W(\boldsymbol{x}-\boldsymbol{x}_j) \tag{2·4}$$

and

$$\langle \boldsymbol{v}(\boldsymbol{x})\rangle=\sum_j m_j \frac{\boldsymbol{v}_j}{\rho_j} W(\boldsymbol{x}-\boldsymbol{x}_j)\,, \tag{2·5}$$

where m_j is the mass of the jth particle, $\rho_j=\rho(\boldsymbol{x}_j)$ and $\boldsymbol{v}_j=\boldsymbol{v}(\boldsymbol{x}_j)$. From Eq. (2·3), we expect the following non-trivial relations to hold:

$$\langle 1\rangle=\sum_j m_j \frac{W(\boldsymbol{x}-\boldsymbol{x}_j)}{\rho_j}=1\,, \tag{2·6}$$

$$\frac{\partial\langle 1\rangle}{\partial x^l}=\sum_j m_j \frac{1}{\rho_j}\frac{\partial}{\partial x^l} W(\boldsymbol{x}-\boldsymbol{x}_j)=0 \tag{2·7}$$

and

$$\frac{\partial^2\langle 1\rangle}{\partial x^\alpha \partial x^\beta}=\sum_j m_j \frac{1}{\rho_j}\frac{\partial^2}{\partial x^\alpha \partial x^\beta} W(\boldsymbol{x}-\boldsymbol{x}_j)=0\,, \tag{2·8}$$

where x^α and x^β are the αth and βth components of the position vector $\boldsymbol{x}$, respectively. These relations will be used in the SPH method to build useful expressions for pressure gradient and viscosity terms. All equations are written in Cartesian coordinates.

The equations to be solved are the equations of motion:

$$\rho\frac{d\boldsymbol{v}}{dt}=\sum_{\alpha,\beta}\boldsymbol{e}_\alpha\frac{\partial}{\partial x^\beta}p^{\alpha\beta}\,, \tag{2·9}$$

where $\boldsymbol{e}_\alpha$ is the unit vector in the αth-coordinate direction. For a fluid which satisfies Stokes' relation, the component of the stress tensor, $p^{\alpha\beta}$, is shown as

$$p^{\alpha\beta}=-p\delta^{\alpha\beta}+\mu\left(\frac{\partial v^\alpha}{\partial x^\beta}+\frac{\partial v^\beta}{\partial x^\alpha}\right)-\frac{2}{3}\mu\delta^{\alpha\beta}\mathrm{div}\,\boldsymbol{v}\,, \tag{2·10}$$

where v^β is the βth component of the velocity $\boldsymbol{v}$, $\delta^{\alpha\beta}$ is Kronecker's delta, μ is the kinematic viscosity and p is the pressure of the fluid. Equation (2·9) is written

$$\frac{d\boldsymbol{v}}{dt}=-\frac{1}{\rho}\nabla p+\frac{\mu}{\rho}\left(\Delta\boldsymbol{v}+\frac{1}{3}\nabla\mathrm{div}\,\boldsymbol{v}\right). \tag{2·11}$$

In SPH, physical quantities for the ith particle are smoothed as

$$\left\langle\frac{d\boldsymbol{v}}{dt}\right\rangle_i=\left\langle-\frac{1}{\rho}\nabla p\right\rangle_i+\left\langle\frac{\mu}{\rho}\left(\Delta\boldsymbol{v}+\frac{1}{3}\nabla\mathrm{div}\,\boldsymbol{v}\right)\right\rangle_i. \tag{2·12}$$

The first term on the right-hand side is approximated as

$$\left\langle-\frac{\nabla p}{\rho}\right\rangle_i=-\frac{1}{\rho_i}\nabla_i\langle p\rangle_i \tag{2·13}$$

and from Eq. (2·3) we have

$$\left\langle-\frac{\nabla p}{\rho}\right\rangle_i=-\frac{1}{\rho_i}\nabla_i\sum_j m_j\frac{p_j}{\rho_j}W(\boldsymbol{x}_i-\boldsymbol{x}_j)=-\sum_j m_j\frac{p_j}{\rho_i\rho_j}\nabla_i W(\boldsymbol{x}_i-\boldsymbol{x}_j)\,. \tag{2·14}$$

To anti-symmetrize the pressure force between each pair of particles, we add to Eq. (2·14) the term

$$-\sum_j m_j \frac{p_i}{\rho_i \rho_j} \nabla_i W(\boldsymbol{x}_i - \boldsymbol{x}_j) = -\frac{p_i}{\rho_i} \nabla_i \sum_j m_j \frac{1}{\rho_j} W(\boldsymbol{x}_i - \boldsymbol{x}_j), \tag{2·15}$$

which is supposed to be zero from Eq. (2·7) (see Miyama[19] and Libersky & Petschek[8]). Then the pressure force term we use is

$$\left\langle -\frac{\nabla p}{\rho} \right\rangle_i = -\sum_j m_j \frac{p_i + p_j}{\rho_i \rho_j} \nabla_i W(\boldsymbol{x}_i - \boldsymbol{x}_j), \tag{2·16}$$

which corresponds to $\sigma=1$ of Eq. 3.6 of Monaghan.[6] The viscous term ${}^{C}\mathcal{V}$, which is the second term on the right-hand side of Eq. (2·11), is approximated as

$$\begin{aligned} {}^{C}\mathcal{V}_i &= \frac{\mu}{\rho_i} \left[\Delta \langle \boldsymbol{v} \rangle + \frac{1}{3} \nabla \mathrm{div} \langle \boldsymbol{v} \rangle \right]_i \\ &= \frac{\mu}{\rho_i} \sum_j \sum_{\alpha,\beta} m_j \frac{\boldsymbol{e}_\beta}{\rho_j} \left[v_j^\beta \frac{\partial^2}{\partial x_i^\alpha \partial x_i^\alpha} + \frac{1}{3} v_j^\alpha \frac{\partial^2}{\partial x_i^\beta \partial x_i^\alpha} \right] W(\boldsymbol{x}_i - \boldsymbol{x}_j). \end{aligned} \tag{2·17}$$

The viscous force is anti-symmetrized by subtracting

$${}^{C}\mathcal{V}'_i = \frac{\mu}{\rho_i} \sum_j \sum_{\alpha,\beta} m_j \frac{\boldsymbol{e}_\beta}{\rho_j} \left[v_i^\beta \frac{\partial^2}{\partial x_i^\alpha \partial x_i^\alpha} + \frac{1}{3} v_i^\alpha \frac{\partial^2}{\partial x_i^\beta \partial x_i^\alpha} \right] W(\boldsymbol{x}_i - \boldsymbol{x}_j) \tag{2·18}$$

from Eq. (2·17). Equation (2·8) implies that ${}^{C}\mathcal{V}'_i=0$, and the final expression for ${}^{C}\mathcal{V}_i$ is

$${}^{C}\mathcal{V}_i = -\frac{\mu}{\rho_i} \sum_j \sum_{\alpha,\beta} m_j \frac{\boldsymbol{e}_\beta}{\rho_j} \left[v_{ij}^\beta \frac{\partial^2}{\partial x_i^\alpha \partial x_i^\alpha} + \frac{1}{3} v_{ij}^\alpha \frac{\partial^2}{\partial x_i^\beta \partial x_i^\alpha} \right] W(\boldsymbol{x}_i - \boldsymbol{x}_j), \tag{2·19}$$

where $v_{ij}^\beta = v_i^\beta - v_j^\beta$. Now, the equation of motion for the ith particle is

$$\begin{aligned} \left\langle m_i \frac{d\boldsymbol{v}_i}{dt} \right\rangle &= -\sum_j m_i m_j \frac{p_i + p_j}{\rho_i \rho_j} \nabla_i W(\boldsymbol{x}_i - \boldsymbol{x}_j) \\ &\quad - \mu \sum_j \sum_{\alpha,\beta} \frac{m_i m_j}{\rho_i \rho_j} \boldsymbol{e}_\beta \left[v_{ij}^\beta \frac{\partial^2}{\partial x_i^\alpha \partial x_i^\alpha} + \frac{1}{3} v_{ij}^\alpha \frac{\partial^2}{\partial x_i^\beta \partial x_i^\alpha} \right] W(\boldsymbol{x}_i - \boldsymbol{x}_j) \\ &\equiv \sum_j \mathcal{P}_{ij} + \sum_j {}^{C}\mathcal{V}_{ij} \equiv \sum_j \boldsymbol{F}_{ij}. \end{aligned} \tag{2·20}$$

If we assume that the kernel W is a function of $r_{ij}=|\boldsymbol{x}_i-\boldsymbol{x}_j|$, then

$$W(\boldsymbol{x}_i - \boldsymbol{x}_j) = W(r_{ij}) \tag{2·21}$$

and

$$\nabla_i W(\boldsymbol{x}_i - \boldsymbol{x}_j) = \frac{\boldsymbol{x}_{ij}}{r_{ij}} \frac{\partial W}{\partial r_{ij}}, \tag{2·22}$$

where $\boldsymbol{x}_{ij}=\boldsymbol{x}_i-\boldsymbol{x}_j$. The pressure gradient force and viscous force exerted on the ith particle by the jth particle, $\mathcal{P}_{ij}$ and ${}^{C}\mathcal{V}_{ij}$, are written as

$$\mathcal{P}_{ij} = -m_i m_j \frac{p_i + p_j}{\rho_i \rho_j} \nabla_i W(\boldsymbol{x}_i - \boldsymbol{x}_j) = -m_i m_j \frac{p_i + p_j}{\rho_i \rho_j} \boldsymbol{x}_{ij} \frac{1}{r_{ij}} \frac{\partial W}{\partial r_{ij}}, \tag{2·23}$$

$${}^{C}\mathcal{V}_{ij} = -\mu \frac{m_i m_j}{\rho_i \rho_j} \left[\boldsymbol{v}_{ij} \left(n + \frac{1}{3} \right) \frac{1}{r_{ij}} \frac{\partial W}{\partial r_{ij}} + \left(\frac{\boldsymbol{v}_{ij} \cdot \boldsymbol{x}_{ij}}{3} \boldsymbol{x}_{ij} + \boldsymbol{v}_{ij} \boldsymbol{x}_{ij}^2 \right) \frac{1}{r_{ij}} \frac{\partial}{\partial r_{ij}} \left(\frac{1}{r_{ij}} \frac{\partial W}{\partial r_{ij}} \right) \right], \tag{2·24}$$

and the forces are anti-symmetric, i.e.,

$$\mathcal{P}_{ji}=-\mathcal{P}_{ij}\,,\qquad \mathcal{V}_{ji}=-\mathcal{V}_{ij} \tag{2·25}$$

and

$$\boldsymbol{F}_{ji}=-\boldsymbol{F}_{ij}\,. \tag{2·26}$$

The law of action and reaction is shown by Eqs. (2·20) and (2·26) and the expressions conserve total momentum exactly.[20]

Consider a volume $\bar{V}$ moving with a fluid. From Eq. (2·9), the time variation of $\boldsymbol{A}$, the total angular momentum of the fluid in the volume, is given by

$$\frac{d\boldsymbol{A}}{dt}=\frac{d}{dt}\int_{\bar{V}}\boldsymbol{x}\times\boldsymbol{v}\rho dV=\int_{\bar{V}}\boldsymbol{x}\times\frac{d\boldsymbol{v}}{dt}\rho dV$$

$$=\int_{\bar{V}}\boldsymbol{x}\times\sum_{\alpha,\beta}\boldsymbol{e}_\alpha\frac{\partial p^{\alpha\beta}}{\partial x^\beta}dV=\sum_{\alpha,\beta}\sum_{\lambda,\mu}\int_{\bar{V}}\epsilon_{\lambda\mu\alpha}\boldsymbol{e}_\lambda\left(\frac{\partial}{\partial x^\beta}x^\mu p^{\alpha\beta}\right)dV\,, \tag{2·27}$$

where $\epsilon_{\lambda\mu\alpha}$ is the unit alternating tensor, and $p^{\alpha\beta}=p^{\beta\alpha}$ is assumed. The equation shows that the time variation of the total angular momentum is given by the surface integral on $\bar{S}$ which surrounds $\bar{V}$. If the integral is zero, the total angular momentum is conserved.

In SPH, an integration is approximated by a summation and the error of the total angular momentum will tend to zero in the limit $h\to 0$, where h is the width of particles shown below. Since the pressure gradient force between two particles is along the line of centers the force does not change the "local" (hence total) angular momentum.[20] But similar considerations do not apply to the viscous force, for its direction is not along the line of centers due to shear stress. The *zero* term Eq. (2·18), which is added to anti-symmetrize the viscous force, will lead to a small amount of error in the total angular momentum.

It will be very difficult to find a numerical method which satisfies both momentum conservation and angular momentum conservation exactly for viscous flows with no symmetries. Even if a numerical scheme is coded as to conserve total angular momentum, it is not guaranteed that the scheme simulates flows without local artificial diffusion of angular momentum. Any scheme must be checked by comparing its results with those of experiments and/or those given by different numerical schemes.

Throughout our numerical simulations, we use a Gaussian kernel:

$$W(\boldsymbol{x}_i-\boldsymbol{x}_j)=\frac{1}{\pi^{n/2}}\frac{1}{2}\left(\frac{e^{-x_{ij}^2/h_i^2}}{h_i^n}+\frac{e^{-x_{ij}^2/h_j^2}}{h_j^n}\right) \tag{2·28}$$

for n-dimensional flow, where $m_j=m_o=$const., $h_i=\eta\Delta_i$ and $\Delta_i=(m_o/\rho_i)^{1/n}$ (or $\Delta_i=(m_o/\rho_o)^{1/n}$ when h is fixed). This kernel is infinitely differentiable and we expect that the second derivatives of it cause no difficulties. Most calculations are performed with $\eta=1.4$, which is expected to give a good velocity field from the estimation by one-dimensional analytic calculation. While the accuracy of numerical simulations by SPH depends *weakly* on the forms of kernel functions, the main factor that

determines the accuracy is the width of the kernel function, h, which is comparable to the mean particle distance Δ_i. Therefore, an increase in the number of particles in the calculation domain will decrease the error of SPH simulation.

The equations for each particle,

$$\frac{d\boldsymbol{x}_i}{dt}=\boldsymbol{v}_i\,, \tag{2·29}$$

$$\frac{d\boldsymbol{v}_i}{dt}=\left(-\frac{1}{\rho}\nabla p\right)_i+\frac{\mu}{\rho_i}\left[\Delta\boldsymbol{v}+\frac{1}{3}\nabla\mathrm{div}\,\boldsymbol{v}\right]_i\,, \tag{2·30}$$

are integrated by the Runge-Kutta-Gill method, with the expression of the right-hand side of Eq. (2·30) shown above. At the end of each time step, the density at the ith particle is calculated by

$$\rho_i=m_o\sum_j W(\boldsymbol{x}_i-\boldsymbol{x}_j)\,, \tag{2·31}$$

and Δ_i is evaluated with ρ_i for the case of variable h. Hereafter, the bracket $\langle\ \rangle$ is not shown for simplicity.

Particular attention should be given to our numerical boundary conditions. In SPH, the densities and velocities of a fluid are given by the superposition of contributions from SPH particles, as shown by Eqs. (2·5) and (2·31). For a particle near a boundary, it is necessary to consider contributions from imaginary particles which are assumed to exist outside the boundary.[3),9)] The details of our boundary conditions are given in Appendix A.

§ 3. Test calculations for viscous flow by our SPH method

Here the method given in the previous section is applied to simulations of two-dimensional Poiseuille flow and Hagen-Poiseuille flow.

3.1. *Two-dimensional Poiseuille flow*

As a first test of SPH calculations for viscous flows, we perform a simulation of a flow between two parallel plates, i.e., two-dimensional Poiseuille flow (plane Poiseuille flow). In this subsection, the x-axis is taken as the flow direction and the y-axis is the direction perpendicular to x (see Fig. 1).

In the configuration shown in Fig. 1, a stationary solution, where the pressure gradient in the x-direction is assumed to be constant, is given by

$$c^2=c_o{}^2-\frac{2\mu_o v_o}{\rho_o r_o{}^2}x\,,\quad p=p_0-\frac{2\mu_o v_o}{r_o{}^2}x\,,\quad \rho=\rho_o\,,$$

$$v_x=v_o\left(1-\frac{y^2}{r_o{}^2}\right),\quad v_y=0\,, \tag{3·1}$$

where c is the sound velocity, μ_o is the coefficient of viscosity and r_o is half the distance between the plates. Here c_o, v_o and ρ_o are constant values. The purpose of our calculation is to test how accurately flow velocity and density, given by (3·1), are obtained using our SPH method.

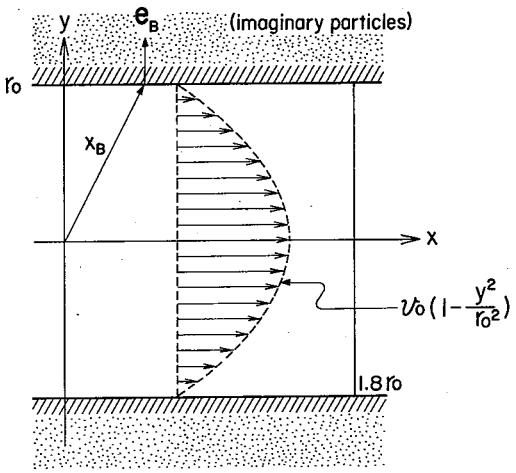

Fig. 1. Configuration of two-dimensional Poiseuille flow between two parallel plates. Velocity vectors are shown at several points along the y-direction. Outside the boundary surface, $|y|>r_o$, we assume the existence of imaginary particles with which we can obtain the proper boundary conditions. The vector e_B is a unit vector perpendicular to the boundary surface and x_B is one of the position vectors at that surface.

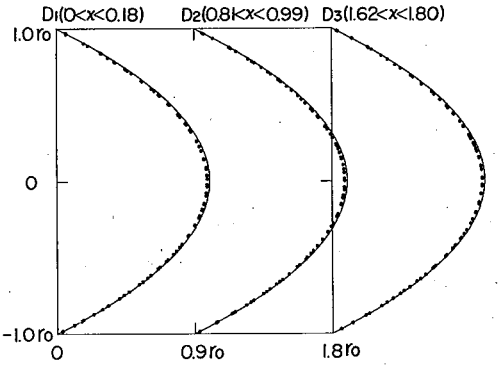

Fig. 2. Results for two-dimensional Poiseuille flow using our SPH method. The smoothed velocities (see Appendix B) of particles in three parts of the calculation region, $D_1=(0<x<0.18r_o)$, $D_2=(0.81r_o<x<0.99r_o)$ and $D_3=(1.62r_o<x<1.80r_o)$ are shown. The positions of dots represent $\boldsymbol{x}_i=x_k\boldsymbol{e}_x+y_i\boldsymbol{e}_y+\boldsymbol{v}_i(r_o/v_0)$. The smoothed velocities (dots) are close to those of analytic solutions (solid curves: parabolas).

For a particle near a boundary, it is necessary to assume the existence of imaginary particles lying outside the calculation region, details of which are given in Appendix A. The distribution of imaginary particles (in $|y|>r_o$) is assumed to be uniform with *local density* ρ_i for the ith particle. Velocities of imaginary particles are assumed to be a linear function of y and vanish at $y=\pm r_o$. Integrated boundary conditions are given in Appendix A. A cyclic boundary condition is applied for the particle distribution in the x-direction.

First, 810 particles are placed randomly in a rectangular region with a size of $1.8r_o$ (x-direction)$\times 2.0r_o$ (y-direction) (see Fig. 1), and all the particles are initially at rest. The mean distance between particles, Δ_o, is $6.67\cdot10^{-2}r_o$ and $m_o=4.44\cdot10^{-3}\rho_o r_o^2$. The smoothing length h is given by $h_i=\eta(m_o/\rho_i)^{1/2}$, and throughout the calculation we set $\eta=1.4$. In this test problem, c_o and μ_0 are set as $c_0=2.0v_o$ (Mach number $M=0.5$) and $\mu_o=0.2r_o v_o\rho_o$.

Although all the particles are initially at rest, they begin to move by virtue of the pressure gradient force. The calculation is performed from $t=0$ to $t=12.0(r_o/v_o)$. The smoothed velocities of the particles in the three parts of the calculation regions $D_1=(0<x<0.18r_o)$, $D_2=(0.81r_o<x<0.99r_o)$ and $D_3=(1.62r_0<x<1.8r_o)$ are shown in Fig. 2. The positions of the dots are

$$\boldsymbol{x}_i=x_k\boldsymbol{e}_x+y_i\boldsymbol{e}_y+\boldsymbol{v}_i(r_o/v_o) \qquad \text{for the } i\text{th particle in } D_k$$

with

$$x_1=0.0\,,\quad x_2=0.9r_o\,,\quad x_c=1.8r_0\,,$$

where $\boldsymbol{e}_x$ and $\boldsymbol{e}_y$ are unit vectors in the x- and y-direction, respectively. The solid lines show the analytic solution: a series of parabolas ($x=(1-y^2/r_o^2)r_o+x_k$, $k=1, 2, 3$). The maximum and minimum calculated densities are $\rho_{\max}=1.009\rho_0$ and $\rho_{\min}=0.994\rho_o$. The result is very close to that of two-dimensional Poiseuille flow.

3.2. *Hagen-Poiseuille flow*

In this subsection, it is shown that our SPH method allows simulation of three-dimensional Poiseuille flow in a circular cylinder, i.e., Hagen-Poiseuille flow. The configuration we consider is shown in Fig. 3, where the x-axis is taken as the flow direction.

In this coordinate system, the Hagen-Poiseuille flow is given as

$$c^2=c_o^2-\frac{4\mu_o v_o}{\rho_o r_o^2}x\,,\quad p=p-\frac{4\mu_o v_o}{r_o^2}x\,,\quad \rho=\rho_o\,,$$

$$v_x=v_o\left(1-\frac{y^2+z^2}{r_o^2}\right),\quad v_y=v_z=0\,. \tag{3·2}$$

We use 19085 particles in a circular cylinder which has the size of $1.8r_o$ (x-direction) $\times 2.0r_o$ (diameter of the cylinder$=2r_o$). At $t=0$, the particles are placed randomly with zero velocities. The magnitudes of Δ_o, m_o, η, ρ_o, c_o and v_0 are the same as those of two-dimensional Poiseuille flow, but $\mu_o=0.1r_o v_o\rho_o$. The smoothing length h is given by $h_i=\eta(m_o/\rho_i)^{1/3}$. Only at the early stage of the calculation, Eq. (B·1) is applied a few times in order to stabilize the calculation. The calculation is performed up to $t=12.0(r_o/v_o)$. The range of the density is $0.995\rho_o\leq\rho\leq 1.002\rho_o$. Figure 4 shows smoothed velocities of the particles in D_k, where $D_1=(0<x<0.04r_o)$, $D_2=(0.88r_o<x<0.92r_o)$ and $D_3=(1.76r_o<x<1.8r_o)$. The obtained

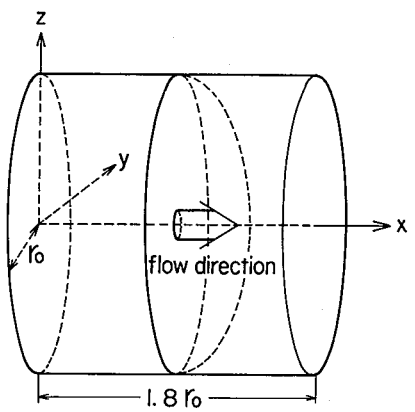

Fig. 3. Configuration of test problem for Hagen-Poiseuille flow in a circular cylinder. Outside the cylinder, $|r|>r_o$, where $r=\sqrt{y^2+z^2}$, there are assumed to be imaginary particles.

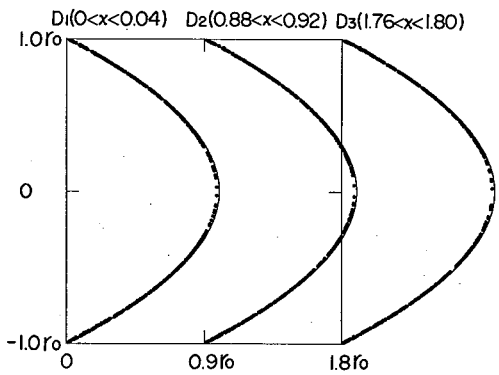

Fig. 4. Results for Hagen-Poiseuille flow using the SPH method. The particles in regions $D_1=(0<x<0.04r_o)$, $D_2=(0.88r_o<x<0.92r_o)$ and $D_3=(1.76r_o<x<1.8r_o)$ are shown. The positions of dots represent $\boldsymbol{x}_i=x_k\boldsymbol{e}_x+(z_i/|z_i|)\sqrt{y_i^2+z_i^2}\,\boldsymbol{e}_y+v_i(r_0/v_0)$ for the ith particle. The smoothed velocities (dots) lie nearly on the parabolas expected from analytic calculation. Because of the cylindrical configuration, the volume element in D_i, $2\pi r dr$, is much smaller in the vicinity of the central axis than near the boundary of the cylinder, and thus fewer particles are seen near the axis.

velocities of the particles are very close to the expected values, i.e., paraboloids. The result suggests that three-dimensional viscous flow can be solved using the SPH method.

§ 4. Flow around a cylinder

Steady incompressible flows around cylinders at moderate Reynolds number have been extensively examined both by experiment[21] and numerical computation.[22)~24)] As mentioned in § 1, however, it is necessary to treat compressible flows in dealing with astrophysical phenomena. Therefore, we have attempted to simulate compressible flow in order to check whether viscous flows can be solved by the SPH method. For the sake of simplicity, isothermal flows are considered in this section.

4.1. *Finite difference method*

Most of the experimental and numerical studies have treated incompressible flows around cylinders. To evaluate the results of SPH by comparison with numerical solutions for the same conditions, we must also simulate isothermal compressible flows by a finite difference method (FDM), namely, an implicit approximate factorization method using inversion of a block pentadiagonal matrix,[16),25)] but the energy equation is neglected in this case.

Here the equation of continuity and the equations of motion are solved implicitly in polar coordinates (r, θ). Assuming mirror symmetry, we use 55 (r)×95 (θ of the upper half plane) grid points (including boundary points), where $r_{\max}=517r_o$ and r_o is the radius of the cylinder. The grid size in the radial direction changes as $\Delta r_i = r_i - r_{i-1} = 1.1\Delta r_{i-1}$ for small i and Δr_i=const. for $i \simeq 95$. In the azimuthal direction, the size changes with $\Delta\theta=\pi/51$.

At the inflow boundary ($r=517r_o$ and $x<0$), $\rho=\rho_o$, $v_x=v_o$, $v_y=0$ and $p_o=c_o^2\rho_o$ are given. At the outflow boundary ($r=517r_o$ and $x>0$), the pressure is fixed as $p=p_o$ (hence $\rho=\rho_o$) and v_x and v_y are given by extrapolation from inner grid points. (Other calculations were performed with boundary conditions given by the solution of Riemann problem[26] at the boundary. The differences between the results are very small.) The calculations are performed for $c_o=2v_o$ (Mach number of the inflow at infinity $M_\infty=0.5$) and $R_e=6$, 10, 20, 30 and 55, where the Reynolds number R_e is defined by

$$R_e=\frac{2r_ov_o}{\mu/\rho_o}=\frac{2r_ov_o}{\nu}. \tag{4·1}$$

4.2. *SPH method*

In our SPH method, Eqs. (2·29) and (2·30) are integrated with respect to time by the Runge- Kutta-Gill method, where p_i is given by $p_i=c_o^2\rho_i$ and c_o is the isothermal sound velocity. For the SPH calculation, unlike the FDM, mirror symmetry is not assumed.

For simulations of isothermal flow around a cylinder with radius r_o and $R_e=6$, we place 46040 particles (case A) or 20462 particles (case B) randomly in the calculation region, region I ($r_o \le r \le 11.7r_o$) (see Fig. 5), with velocities $v_{xi}=v_o$ and $v_{yi}=0$. Inflow

particles are placed on grid points ($\Delta x_i = \Delta y_j = \Delta_o$) in the region upstream of the calculation region. The particles flow into region II ($11.7r_o < r \leq 12.4r_o$ and $x \leq 0$) (see Fig. 5) and the particles in this region express the inflow boundary condition. These particles flow with constant velocities and constant densities, which are given at $r = 12.4r_o$ by the results obtained from the calculations by the FDM, until they reach region I or region III ($11.7r_o < r \leq 12.4r_o$ and $0 < x$). These boundary values given by the FDM are dependent on the coefficient of viscosity μ. The smoothing length is given by $h = \eta(m_o/\rho_o)^{1/2}$.

In region III, particles flow out with the velocities that were fixed after they entered this region from I or II. The pressure (hence the density) at the particle's position in III is given by the values (at $r = 12.4r_o$) obtained by the FDM.

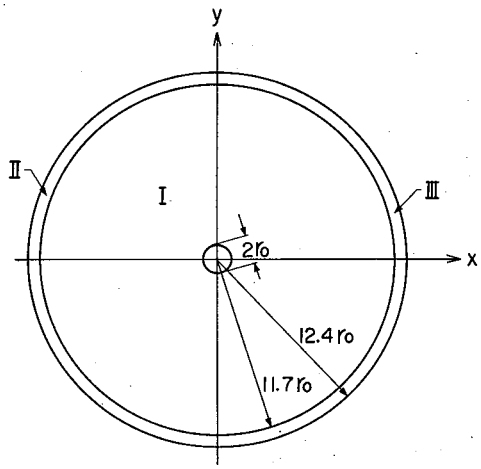

Fig. 5. Calculation region for the flow around a cylinder using the SPH method. The radius of the cylinder is r_o. The particles in the region I ($r_o \leq r \leq r_1 = 11.7r_o$) are calculated by the SPH method. The particles in the region II ($r_1 \leq r \leq r_2 = 12.4r_o$, $x \leq 0$) are inflowing boundary particles and the particles in III ($r_1 \leq r \leq r_2$, $0 \leq x$) are outflowing boundary particles.

Our numerical simulation is intended primarily to test whether viscous flows around a cylinder can be solved by our SPH method, and we do not, therefore, need to be overly concerned with the inflow and outflow boundary conditions. In the FDM, the inflow and outflow boundaries can be set at larger distances than in the SPH calculation. For simplicity, therefore, the results of the FDM calculations are used as the boundary values of the SPH calculations.

When the calculation is continued over several crossing times (diameter of the calculation region/inflow velocity), we find that the variation in the drag coefficients of the cylinder (defined in Appendix C) diminishes and the flow attains nearly a steady state. The lift on the cylinder becomes small though it oscillates with a small amplitude. Once the steady state is obtained for one model, the Reynolds number is raised and the calculation is continued with new boundary values to get a new steady state. We repeat these processes and obtain results for $R_e = 6$, 10, 20, 30 and 55 for both Cases A and B. In the early steps, velocities are smoothed several times by Eq. (B·1) in order to avoid velocity amplification. Consequently, the calculations are stable over several crossing times.

4.3. *Results of the calculations*

As a typical case of the flows, we describe in detail the results for $R_e = 20$.

Figure 6(a) shows the density contours of the results with our SPH method. The lines are almost symmetric with respect to $y = 0$. The results of calculation by the FDM, assuming mirror symmetry about $y = 0$, are shown in Fig. 6(b). The coincidence of the two figures suggests that the two numerical methods give nearly the same

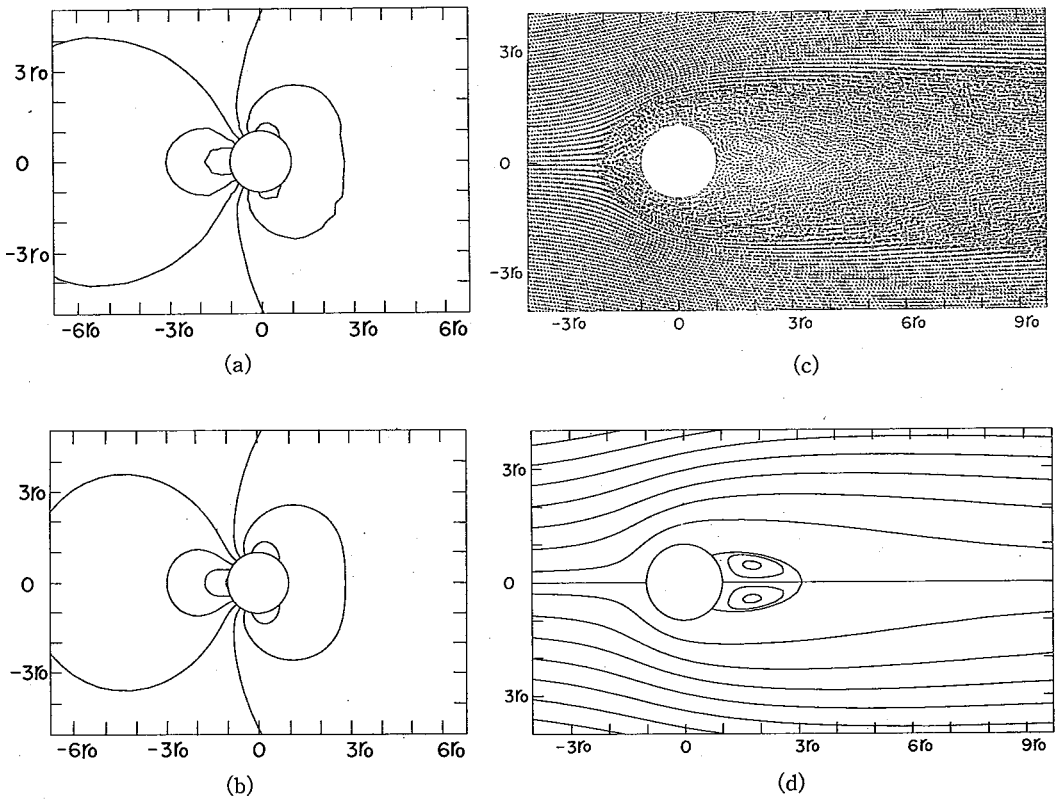

Fig. 6. Density contours and velocity fields for isothermal flows around a cylinder at $R_e=20$, where contour levels are, in ρ_o unit, 0.8938, 0.9375, 0.9813, 1.025, 1.069 and 1.113. (a) is the result with the SPH method and (b) is that with the FDM. (c) shows the velocities of the particles calculated by the SPH method. The positions of the particles are in the middle of the arrows. (d) shows stream lines of the flow calculated by the FDM. The two flow patterns, including the size of circulation regions behind the cylinder, coincide well.

results.

The velocity field near the cylinder is compared in Figs. 6(c) and (d). The arrows in (c) show the direction of the particle velocity. The length of the arrow of the ith particle is proportional to $1/\{1-\log(v_i/v_{\max})\}$, where v_i is the magnitude of the velocity and $v_{\max}$ is the largest of the particle velocities. The position of a particle is in the middle of the arrow. Figure 6(d) shows stream lines calculated by the FDM. Comparison of these two figures shows that both calculations give almost the same flow fields. Lengths of separated regions and separation angles obtained by the two simulations nearly coincide. The results are almost the same as those for incompressible flow around a cylinder.[21)~23)]

The Reynolds number $R_e=6$ is the critical value at which separated regions appear behind a cylinder.[21),23)] In our calculation no clear circulations are observed (see Fig. 7). The result for $R_e=10$ shows symmetric circulation flows (see Fig. 8). These become larger as the Reynolds number increases (see Figs. 6~10). Both the flow patterns and the sizes of the circulation regions obtained using the two methods coincide well. The flow fields obtained by SPH for $R_e=55$ are slightly asymmetric,

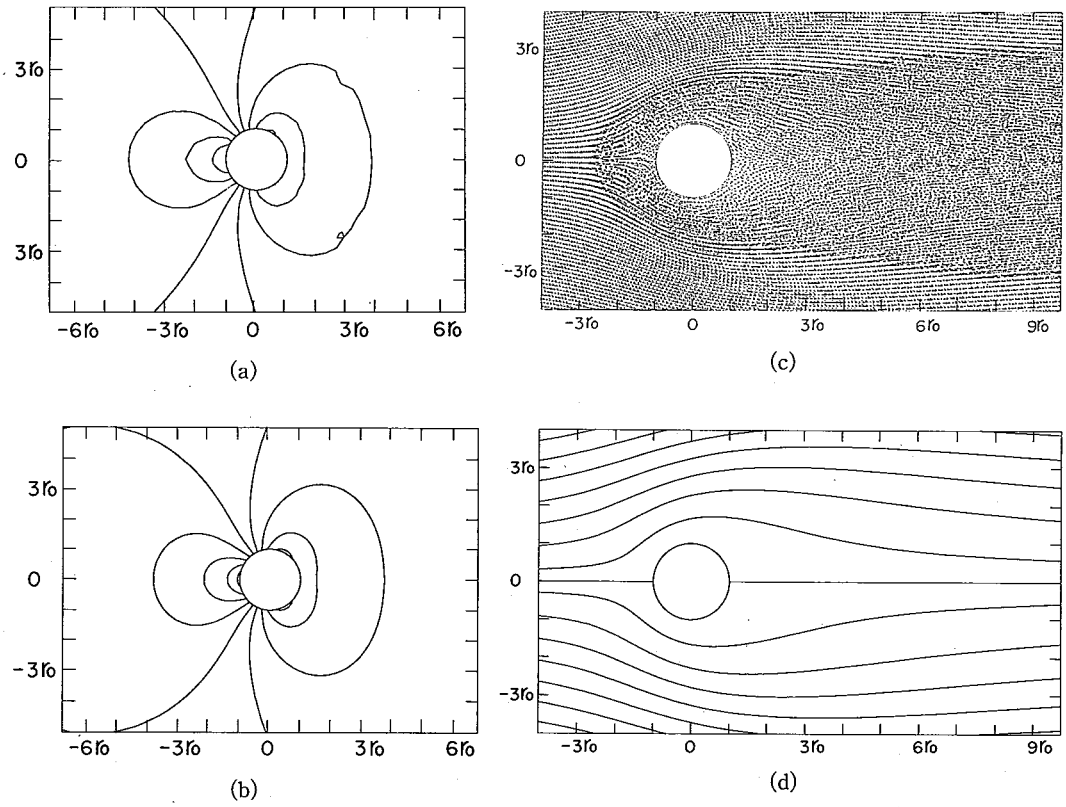

Fig. 7. Density contours and velocity fields for isothermal flows around a cylinder at $R_e=6$, where contour levels are, in ρ_o unit, 0.850, 0.8938, 0.9375, 0.9813, 1.025, 1.069, 1.113, 1.156 and 1.200. This Reynolds number is the critical value at which circulations appear behind the cylinder.

as is expected from experimental and numerical studies.[21),23)] The density contours obtained by SPH are very close to those obtained by the FDM for $R_e=6\sim55$ (see density contours of Figs. 6~10). The density profiles and velocity fields of Case B (not shown here) are almost the same as those of Case A, though the contour lines of Case B are slightly less smooth.

Table I shows the values of the three drag coefficients, where C_t, C_p and C_v are total, pressure and viscous drag coefficient, respectively (see Appendix C). Table I(a) lists the results obtained from the FDM, and Tables I(b) and (c) present the results of the SPH method for Case A and Case B, respectively. The total drag coefficients obtained by SPH (Cases A and B) for $R_e=6\sim30$ agree with those obtained by the FDM within errors of 2~3 %, and it is shown that the results of Case A is better than those of Case B. The values of the drag coefficients are almost the same as those of incompressible flow.[22),24)]

For $R_e=55$, the detached region behind the cylinder is of comparable size to the radius of the calculation region. We expect that the larger calculation region will improve the results. The order of the width of the boundary layer, estimated from $r_o/\sqrt{R_e}=r_o/\sqrt{55}\sim0.135r_o$, is smaller than $\Delta_o=0.144r_o$ for Case B. Though the resolution seems insufficient for this calculation, the magnitude of the error is only

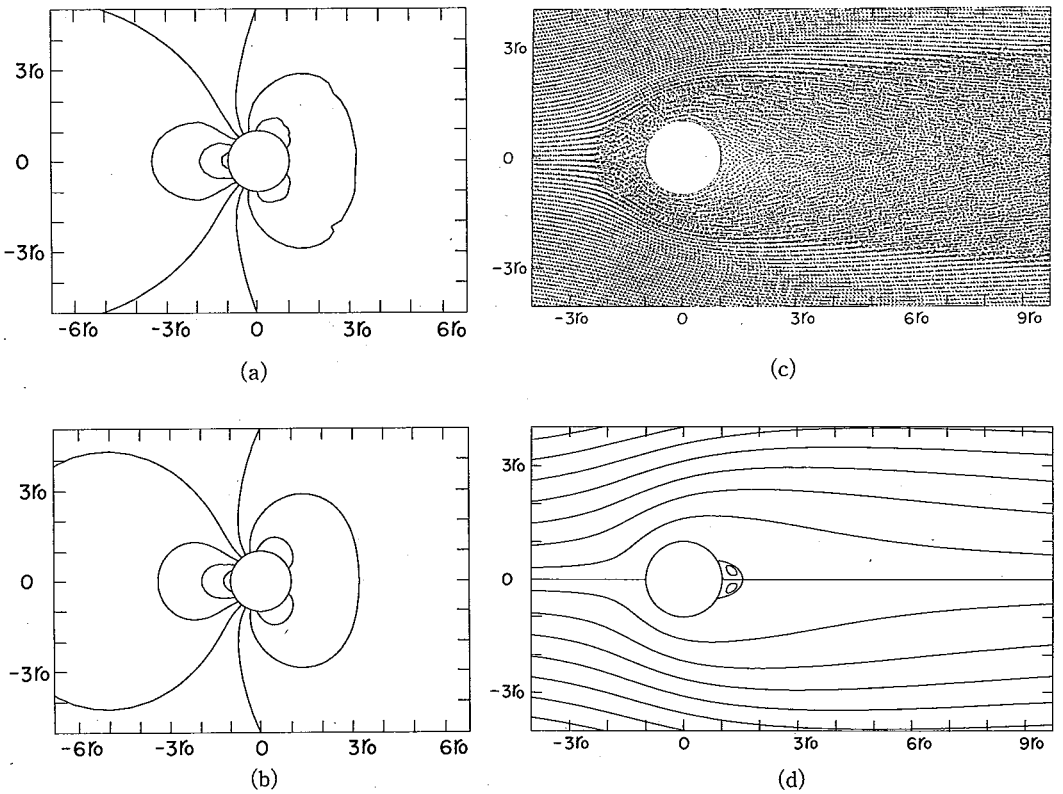

Fig. 8. Density contours and velocity fields for isothermal flows around a cylinder at $R_e=10$, where contour levels are, in ρ_o unit, 0.8938, 0.9375, 0.9813, 1.025, 1.069, 1.113 and 1.156.

Table I. Drag coefficients. R_e is the Reynolds number, C_t the total drag coefficient, C_p the pressure drag coefficient and C_v the viscous drag coefficient (defined in Appendix C). FDM lists the results for the finite difference method, SPH (Case A) the SPH method with 46040 initial particles and SPH (Case B) the SPH method with 20462 initial particles.

Ia FDM				Ib SPH (Case A)				Ic SPH (Case B)			
R_e	C_t	C_p	C_v	R_e	C_t	C_p	C_v	R_e	C_t	C_p	C_v
6	3.744	2.047	1.697	6	3.80	2.07	1.72	6	3.85	2.10	1.75
10	2.910	1.663	1.247	10	2.96	1.70	1.26	10	2.97	1.70	1.27
20	2.129	1.312	0.8176	20	2.17	1.35	0.818	20	2.19	1.37	0.820
30	1.799	1.164	0.6350	30	1.84	1.21	0.633	30	1.85	1.24	0.616
55	1.423	0.9924	0.4303	55	1.48	1.05	0.431	55	1.52	1.07	0.452

about 8 %.

Calculations hitherto were performed with $\eta=1.4$. To check the effect of this value, additional calculations were done with $\eta=1.3$ and 1.2 for $R_e=20$. Drag coefficients (C_t, C_p, C_v) are (2.18, 1.35, 0.824) for $\eta=1.3$ and (2.20, 1.37, 0.830) for $\eta=1.2$. We expect that simulations with an η value of 1.2~1.4 to give good results. The drag coefficients obtained by the SPH method are the mean values of their local maximum and minimum values at the late stage of calculation.

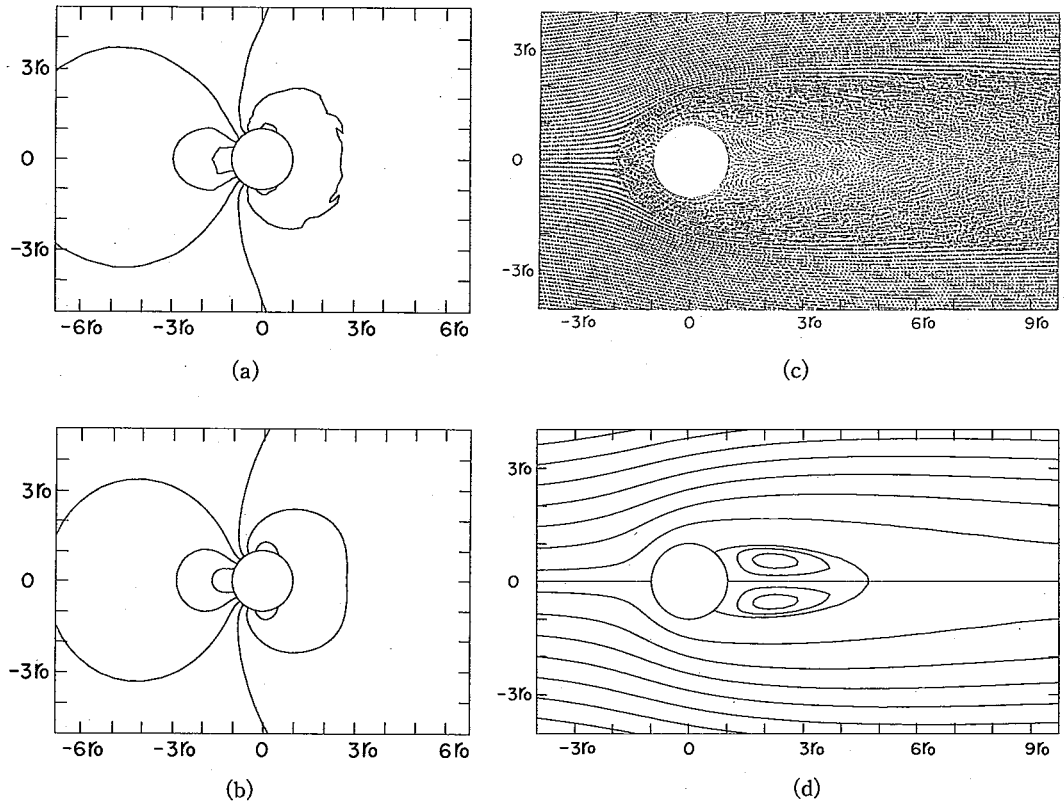

Fig. 9. Density contours and velocity fields for isothermal flows around a cylinder at $R_e=30$, where contour levels are, in ρ_o unit, 0.8938, 0.9375, 0.9813, 1.025, 1.069 and 1.113. Two circulations are clearly seen.

It is not essential to fix the value of h for the simulation of viscous flows around a cylinder. For $R_e=20$ and $\eta=1.4$, another calculation with variable h, $h_i=\eta(m_o/\rho_i)^{1/2}$, was performed. We obtained a similar result to that with fixed h and drag coefficients of (2.17, 1.33, 0.844).

§ 5. Summary

The extension of the SPH method is straightforward even in the case of the Navier-Stokes equations, which include second-order derivatives with respect to the position of particles.

When the method was applied to two-dimensional Poiseuille flow, it was found that only about 1000 particles are sufficient to simulate the viscous flow. It was also applied to three-dimensional flow in a circular cylinder: Hagen-Poiseuille flow. The velocities and densities of the particles agreed well with those of the analytic solutions.

Isothermal viscous flows around a cylinder were also simulated using the SPH method for $R_e=6$, 10, 20, 30 and 55 with initial particle numbers 20462 and 46040. The results were compared with the mirror-symmetric isothermal flows obtained from

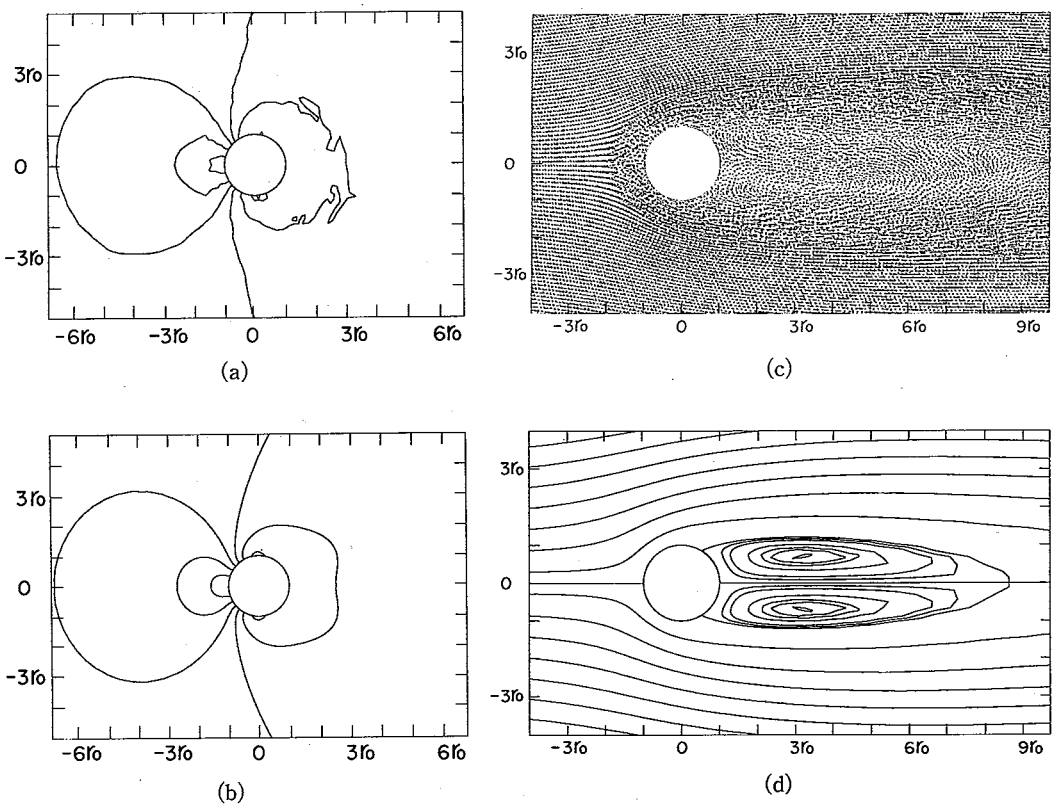

Fig. 10. Density contours and velocity fields for isothermal flows around a cylinder at R_e=55, where contour levels are, in ρ_o unit, 0.8938, 0.9375, 0.9813, 1.025, 1.069 and 1.113, which are the same as those of R_e=30.

calculation by the FDM. The agreement in the drag coefficients is excellent and both methods and experiments give almost the same lengths of circulations and separation angles. Therefore, we consider that the angular momentum transfer is solved correctly by our SPH method.

The Reynolds number of our simulations is not so high, however, the possible Reynolds number increases proportional to particle number N (for two dimensional flow) and to $N^{2/3}$ (for three dimensional flow). Therefore, if calculations are performed with 100 times the particles used in the present calculations, simulations of flows of $R_e \sim 1000-5000$ are possible then the applications of our method to astrophysical problems will be straightforward. Such computations will very soon be possible in the case of non-self-gravitating systems.

Our calculations indicate that the SPH method allows solution of fluid flow equations with second-order derivatives with respect to positions of particles. (According to Brookshaw,[18] his method is applicable to kernels which do not have second order derivatives.) We have not tested viscous flows with shock waves. For such flows, artificial viscosity terms[19),27] should be added to our equations or a scheme such as that of Inutsuka[13] should be combined with our scheme.

This paper shows the results of test calculations only for fundamental viscous

flows which could be simulated by finite difference methods with better accuracy and with less cpu time. As described in the Introduction, however, SPH offers advantages over FDMs. It is shown that the SPH method is applicable even to the Navier-Stokes equations, thus opening further possibilities of applying SPH to numerical simulations. The SPH method developed here can be applied to the viscous flows in laboratories such as flows around moving bodies, as well as in astrophysical circumstances, e.g., accretion disk problems, evolution of planetesimals in proto-solar nebulae and interactions between traveling galaxies and intergalactic medium.

Acknowledgements

We are grateful to Emeritus Professor C. Hayashi and Professor T. Sakurai for valuable discussions. H. T. thanks the National Astronomical Observatory (Nobeyama and Mitaka) for allowing the use of their computers and for their hospitality. Some of the calculations were performed with computers at the Kyoto University Data Processing Center. This work was partly supported by a Grant-in-Aid for Scientific Research No. C-03640248.

Appendix A

—— Boundary Conditions on a Rigid Body ——

This appendix describes details of the boundary conditions on a rigid body used in our SPH method. In SPH calculation to solve the equations for a particle, i.e., to calculate physical quantities of a particle, contributions from particles in the vicinity of that particle must be known. In the case of a rigid body boundary, we must take into consideration the fact that although the velocity of the fluid is zero, the density does not reduce to zero at the boundary surface. That is, for particles near the boundary, the contributions from particles only inside the boundary surface do not give the correct density or velocity. Figure A. 1 illustrates the effect of the rigid boundary for the case of uniform density distribution. In our SPH method, we assume the existence and motion of "imaginary particles" outside the boundary surface and use these particles to specify the boundary conditions required in various physical situations (the "imaginary particles" correspond to

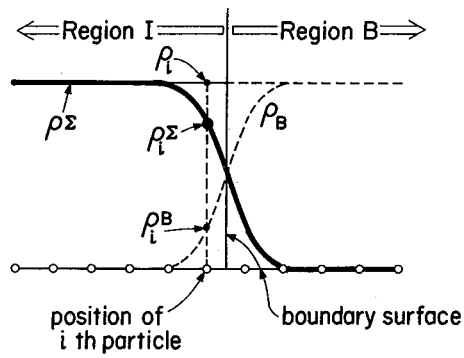

Fig. A.1. Effects of the existence of a boundary on the density calculation for the case of uniform density distribution of SPH particles inside the boundary. The solid curve, ρ^Σ, represents the density given by the sum of the contributions of particles inside the boundary surface. Although the particles inside the boundary (Region I) are uniformly distributed, the value of ρ^Σ is less than the uniform density near the boundary surface. The dashed curve, ρ^B, represents the density contribution from imaginary particles which would exist outside the boundary surface (Region B) if the boundary was absent. Therefore, at the position of the ith particle, the density is assumed to be given by the sum of both densities, as $\rho_i=\rho_i^\Sigma+\rho_i^B$.

ghost particles of Libersky et al.[9]). We call the region inside the boundary surface Region I and the region outside the surface Region B. In Regions I and B there are real and "imaginary" particles, respectively.

Here we evaluate the contributions from imaginary particles to the expressions for physical quantities of the particles near the boundary. The density of the ith particle is given by the sum

$$\rho_i=\rho_i^{\Sigma}+\rho_i^{B}, \tag{A·1}$$

where ρ_i^{Σ} is the contribution from the particles in Region I. For the case of n-dimensional space, Eqs. (2·28) and (2·31) lead to

$$\rho_i^{\Sigma}=\frac{m_o}{\pi^{n/2}}\sum_{j\in I}\frac{1}{2}\left(\frac{e^{-x_{ij}^2/h_i^2}}{h_i^n}+\frac{e^{-x_{ij}^2/h_j^2}}{h_j^n}\right). \tag{A·2}$$

The density ρ_i^{B} is the contribution from imaginary particles. As shown in Fig. A.1, the imaginary particles are assumed to be disributed uniformly with local density ρ_i in Region B. In the case of plane boundary, ρ_i^{B} is given by

$$\rho_i^{B}=\frac{m_o}{\pi^{n/2}}\sum_{j\in B}\frac{e^{-x_{ij}^2/h_i^2}}{h_i^n}=\frac{\rho_i}{\pi^{n/2}}\int_{r_0}^{\infty}\int_{-\infty}^{\infty}\frac{e^{-x_{ij}^2/h_i^2}}{h_i^n}d\boldsymbol{x}_j=\frac{\rho_i}{2}\operatorname{erfc}(t_{oi}). \tag{A·3}$$

Here

$$\operatorname{erfc}(z)=\frac{2}{\sqrt{\pi}}\int_z^{\infty}e^{-t^2}dt, \tag{A·4}$$

$$t_{oi}=\frac{|(\boldsymbol{x}_i-\boldsymbol{x}_B)\cdot\boldsymbol{e}_B|}{h_i} \tag{A·5}$$

and

$$r_o=\boldsymbol{x}_B\cdot\boldsymbol{e}_B, \tag{A·6}$$

where $\boldsymbol{x}_B$ and $\boldsymbol{e}_B$ are a position vector of the boundary surface and a unit vector perpendicular to the surface (see Fig. 1).

From Eqs. (A·1) and (A·3), we obtain a new expression for the density of a particle near the boundary:

$$\rho_i=\rho_i^{\Sigma}/\left(1-\frac{1}{2}\operatorname{erfc}(t_{oi})\right). \tag{A·7}$$

The expression (A·7) is a new formalism which includes the contribution from the imaginary particles. This is our boundary condition for density.

Similar consideration of pressure gradient gives

$$\left(-\frac{\nabla p}{\rho}\right)_i=\left(-\frac{\nabla p}{\rho}\right)_i^{\Sigma}+\left(-\frac{\nabla p}{\rho}\right)_i^{B}. \tag{A·8}$$

The terms on the right-hand side are shown as

$$\left(-\frac{\nabla p}{\rho}\right)_i^{\Sigma}=\frac{m_o}{\pi^{n/2}}\sum_{j\in I}\frac{p_i+p_j}{\rho_i\rho_j}\boldsymbol{x}_{ij}\left(\frac{e^{-x_{ij}^2/h_i^2}}{h_i^{n+2}}+\frac{e^{-x_{ij}^2/h_j^2}}{h_j^{n+2}}\right), \tag{A·9}$$

$$\left(-\frac{\nabla p}{\rho}\right)_i^B=\frac{\lambda}{2}\,\mathrm{erfc}(t_{oi})\boldsymbol{e}_x-\frac{2c_i^2}{\sqrt{\pi}h_i}e^{-t_{oi}^2}\boldsymbol{e}_B\,, \tag{A·10}$$

where $\boldsymbol{e}_x$ is the unit vector along the flow direction (see Fig. 1, Eqs. (A·2) and (A·3)). The first term on the right-hand side of Eq. (A·10) arises from the temperature gradient, dc^2/dx ($\equiv\lambda$). Hence, in the case of two-dimensional Poiseuille flow or Hagen-Poiseuille flow, the value of λ is calculated with Eq. (3·1) or Eq. (3·2). In the case of the flow around a cylinder, we assume an isothermal flow: $\lambda=0$. The proper boundary conditions might be given by combination of pressure and viscosity terms[15),16)] but we leave calculation for the future, with the expectation of more accurate results.

We assume that the velocity distribution of the imaginary particles depends only on the distance from the boundary plane r, as

$$\boldsymbol{v}_j=\boldsymbol{v}_i\frac{r_{oj}}{r_{oi}}=-\boldsymbol{v}_i\frac{r_j-r_o}{r_o-r_i}\,. \tag{A·11}$$

Then the velocity of the particle at the boundary $r_j=r_o$ vanishes, which is consistent with the no-slip condition on the wall. The viscous force is given by

$$\mathcal{V}_i=\mathcal{V}_i^{\Sigma}+\mathcal{V}_i^{B}\,, \tag{A·12}$$

where

$$\mathcal{V}_i^{\Sigma}=\frac{\mu}{\rho_i}\frac{m_o}{\pi^{n/2}}\sum_{j\in I}\frac{1}{\rho_j}\left[\frac{e^{-x_{ij}^2/h_i^2}}{h_i^{n+2}}\left\{\left(n+\frac{1}{3}\right)\boldsymbol{v}_{ij}-\frac{2}{h_i^2}\left(\frac{\boldsymbol{v}_{ij}\cdot\boldsymbol{x}_{ij}}{3}\boldsymbol{x}_{ij}+\boldsymbol{v}_{ij}x_{ij}^2\right)\right\}\right.$$
$$\left.+\frac{e^{-x_{ij}^2/h_j^2}}{h_j^{n+2}}\left\{\left(n+\frac{1}{3}\right)\boldsymbol{v}_{ij}-\frac{2}{h_j^2}\left(\frac{\boldsymbol{v}_{ij}\cdot\boldsymbol{x}_{ij}}{3}\boldsymbol{x}_{ij}+\boldsymbol{v}_{ij}x_{ij}^2\right)\right\}\right], \tag{A·13}$$

$$\mathcal{V}_i^{B}=-\frac{\mu}{\rho_i}\frac{1}{\sqrt{\pi}h_i^2}\frac{2t_{oi}^2+1}{t_{oi}}\left(\boldsymbol{v}_i+\frac{1}{3}v_i^B\boldsymbol{e}_B\right)e^{-t_{oi}^2}\,. \tag{A·14}$$

In the following, we give notes on each of the test problems.

A.1. *Two-dimensional Poiseuille flow*

The boundaries are planes of $y=\pm r_o$ and the unit vectors perpendicular to the planes are $\boldsymbol{e}_B=\pm\boldsymbol{e}_y$ (see Fig. 1).

A.2. *Hagen-Poiseuille flow in a circular cylinder*

The effect of a curved boundary wall is not easily evaluated as the case of a plane boundary. If h (hence Δ_o: mean distance between particles) is much smaller than the radius of the curvature of the wall, $R=r_o$, the effect on the ith particle near the wall will not much be different from that of a plane wall.

For the ith particle, the cylinder wall is approximated with a plane wall Π_i (see Fig. A.2). Hence the expression of the boundary effect on the particle is the same as that of two-dimensional Poiseuille flow if we consider variables are those of three-dimensional space with $n=3$, $\boldsymbol{e}_B$ is a unit vector perpendicular to the cylinder (hence to the plane) and v_i^B is the velocity component in $\boldsymbol{e}_B$ direction.

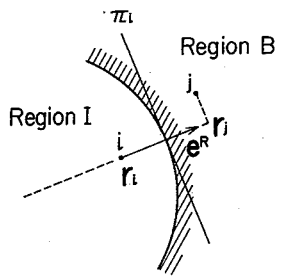

Fig. A.2. View of the boundary for the case of Hagen-Poiseuille flow. The outer boundary surface (cylinder surface) is approximated by the plane Π_i for the ith particle. Density and velocity of the jth imaginary particle are assumed to be $\rho_j=\rho_i$ and $\boldsymbol{v}_j=-\boldsymbol{v}_i\cdot(r_j-r_o)/(r_o-r_i)$.

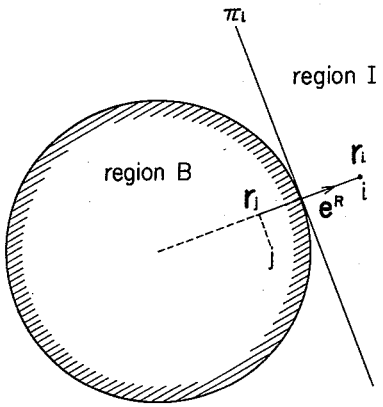

Fig. A.3. View of the boundary for the case of flow around a cylinder. The cylinder surface is approximated by the plane Π_i for the ith particle. Density and velocity of the jth imaginary particle are assumed as shown in the case of Hagen-Poiseuille flow.

A.3. *Flow around a cylinder*

In order that the calculation be simple, we assume that the flow is isothermal (hence $|\nabla c^2|\equiv\lambda=0$ and $c_i=c_j=c_o=$constant) and the equations in the two-dimensional space are solved. For the ith particle near the cylinder, the surface of the boundary is approximated by a plane, Π_i, which contacts with the cylinder (see Fig. A.3).

Appendix B

—— *Smoothed Velocity in the SPH Method* ——

The illustration of velocity fields shows the arrows of smoothed velocities $\tilde{\boldsymbol{v}}_i$, which are given as

$$\tilde{\boldsymbol{v}}_i=\boldsymbol{v}_i+\delta\boldsymbol{v}_i\,, \tag{B·1}$$

where

$$\delta\boldsymbol{v}_i\equiv\sum_j m_j\left[\frac{\boldsymbol{v}_j}{\rho_j}-\frac{\boldsymbol{v}_i}{\rho_i}\right]W(\boldsymbol{x}_i-\boldsymbol{x}_j)\,. \tag{B·2}$$

From Eqs. (2·4) and (2·5), we obtain

$$\delta\boldsymbol{v}_i=\sum_j m_j\frac{\boldsymbol{v}_j}{\rho_j}W(\boldsymbol{x}_i-\boldsymbol{x}_j)-\frac{\boldsymbol{v}_i}{\rho_i}\sum_j m_jW(\boldsymbol{x}_i-\boldsymbol{x}_j)=\langle\boldsymbol{v}\rangle_i-\frac{\boldsymbol{v}_i}{\rho_i}\cdot\langle\rho\rangle_i\cong 0\,. \tag{B·3}$$

The zero term $\delta\boldsymbol{v}_i$ is added to $\boldsymbol{v}_i$ to obtain $\tilde{\boldsymbol{v}}_i$. A similar form is used by Monaghan[20] in the expression of particle velocities, $d\boldsymbol{r}_i/dt$.

If we multiply (B·1) by m_i, we have

$$m_i\tilde{\boldsymbol{v}}_i=m_i\boldsymbol{v}_i+\sum_j m_im_j\left[\frac{\boldsymbol{v}_j}{\rho_j}-\frac{\boldsymbol{v}_i}{\rho_i}\right]W(\boldsymbol{x}_i-\boldsymbol{x}_j)\,. \tag{B·4}$$

For the kernel which satisfies $W(\boldsymbol{x}_i-\boldsymbol{x}_j)=W(r_{ij})$, it is shown that the above process conserves the momentum of the system of SPH particles.

The smoothing process, Eq. (B·1), stabilizes some of the velocity fluctuations. For example, consider a one-dimensional distribution where position of particles are $x_n=n\cdot\Delta x$ and velocities are $v(x_n)=v_n=v_o(-1)^n$ and $\rho=$const. Though the velocity field is enhanced by the viscous force, it is easy to see that the velocity field is smoothed out (hence stabilized) by the processs (B·1).

In the case of smoothed velocity, as in Appendix A, the effect of the boundary is given by

$$\tilde{\boldsymbol{v}}_i=\boldsymbol{v}_i+\delta\boldsymbol{v}_i^{\Sigma}+\delta\boldsymbol{v}_i^{B}\,, \tag{B·5}$$

where

$$\delta\boldsymbol{v}_i^{\Sigma}=\frac{m_o}{\pi^{n/2}}\sum_{j\in I}\left(\frac{\boldsymbol{v}_j}{\rho_j}-\frac{\boldsymbol{v}_i}{\rho_i}\right)\frac{1}{2}\left(\frac{e^{-x_{ij}^2/h_i^2}}{h_i^n}+\frac{e^{-x_{ij}^2/h_j^2}}{h_j^n}\right). \tag{B·6}$$

A simple integration gives

$$\delta\boldsymbol{v}_i^{B}=-\frac{\tilde{\boldsymbol{v}}_i}{2}\frac{1}{\sqrt{\pi}\,t_{oi}}e^{-t_{\delta i}^2}\,, \tag{B·7}$$

where we assume the velocity of the ith particle to be $\tilde{\boldsymbol{v}}_i$ instead of $\boldsymbol{v}_i$. Then we obtain

$$\tilde{\boldsymbol{v}}_i=\frac{\boldsymbol{v}_i+\delta\boldsymbol{v}_i^{\Sigma}}{1+\dfrac{1}{2\sqrt{\pi}\,t_{oi}}e^{-t_{\delta i}^2}}. \tag{B·8}$$

To smooth the velocity means to replace the velocity $\boldsymbol{v}_i$ with the velocity $\tilde{\boldsymbol{v}}_i$.

Appendix C

—— *Drag Coefficients* ——

The force of the fluid on the region which is enclosed by the surface S, is written as

$$\boldsymbol{F}=\iint_S\boldsymbol{p}_n dS=\iint_S\sum_{\alpha,\beta}\boldsymbol{e}_\alpha p^{\alpha\beta}n_\beta dS=\iiint_V\sum_{\alpha,\beta}\boldsymbol{e}_\alpha\left(\frac{\partial}{\partial x^\beta}p^{\alpha\beta}\right)dV\,, \tag{C·1}$$

where $\boldsymbol{p}_n$ is the stress vector, $(p^{\alpha\beta})$ is the stress tensor (2·10) for the fluid with Stokes' relation, $\boldsymbol{n}$ is the unit vector perpendicular to S, V is the volume surrounded by S and α and β show coordinate directions.

We assume that the rigid body is filled with imaginary fluid particles. Then the integration in Eq. (C·1) is approximated by the sum over the imaginary particles in the body (region B),

$$\boldsymbol{F}=\sum_{j\in B}\sum_{\alpha,\beta}\frac{m_j}{\rho_j}\left(\boldsymbol{e}_\alpha\frac{\partial}{\partial x^\beta}p^{\alpha\beta}\right)_j=\sum_{j\in B}\sum_{i\in(I+B)}\boldsymbol{F}_{ji}\,. \tag{C·2}$$

With $F_{ij}\equiv\mathcal{P}_{ij}+\mathcal{V}_{ij}$, the force exerted on the ith particle in the calculation region by the imaginary particle is shown as

$$\sum_{j\in B}\boldsymbol{F}_{ij}=m_i\left[\left(-\frac{1}{\rho_i}\nabla p\right)_i^B+\mathcal{V}_i^B\right]. \tag{C·3}$$

With anti-symmetry of the force,

$$\boldsymbol{F}_{ji}=-\boldsymbol{F}_{ij}\,, \tag{C·4}$$

the force on the body, $\boldsymbol{F}$, is shown as

$$\boldsymbol{F}=\sum_{j\in B}\sum_{i\in(I+B)}\boldsymbol{F}_{ji}=\sum_{j\in B}\sum_{i\in I}\boldsymbol{F}_{ji}+\sum_{j\in B}\sum_{i\in B}\boldsymbol{F}_{ji}=\sum_{j\in B}\sum_{i\in I}\boldsymbol{F}_{ji}=\sum_{i\in I}\Big(-\sum_{j\in B}\boldsymbol{F}_{ij}\Big)\,. \tag{C·5}$$

The force is divided into two parts, the drag on the body by pressure force and the drag by viscous force:

$$\boldsymbol{F}=\boldsymbol{F}_{\mathrm{pres}}+\boldsymbol{F}_{\mathrm{vis}}\,. \tag{C·6}$$

After integration, the drag forces are shown as

$$\boldsymbol{F}_{\mathrm{pres}}=\sum_{i\in I}m_i\Big(\frac{1}{\rho_i}\nabla p\Big)_i^B=-\frac{2{c_o}^2}{\sqrt{\pi}\,h_i}\sum_{i\in I}m_i e^{-t_{oi}^2}\frac{\boldsymbol{x}_i}{r_i}\,, \tag{C·7}$$

$$\boldsymbol{F}_{\mathrm{vis}}=-\sum_{i\in I}m_i{\mathcal{V}_i}^B=\frac{\mu}{\sqrt{\pi}}\sum_{i\in I}m_i\frac{1}{\rho_i{h_i}^2}\frac{2t_{oi}^2+1}{t_{oi}}e^{-t_{oi}^2}\Big[\boldsymbol{v}_i+\frac{\boldsymbol{v}_i\cdot\boldsymbol{x}_i}{3r_i}\frac{\boldsymbol{x}_i}{r_i}\Big]\,. \tag{C·8}$$

Drag coefficients for the cylinder with a radius r_o are written as

$$C_t=F^x/(\rho_o{v_o}^2r_o)\,,\quad C_p=F^x_{\mathrm{pres}}/(\rho_o{v_o}^2r_o)\,,\quad C_v=F^x_{\mathrm{vis}}/(\rho_o{v_o}^2r_o)\,, \tag{C·9}$$

where superscript x denotes the x-component of the forces, C_t is the total drag coefficient, C_p is the pressure drag coefficient, C_v is the viscous drag coefficient, ρ_o is the inflow density and v_o is the inflow velocity.

References

1) L. B. Lucy, Astron. J. **82** (1977), 1013.
2) R. A. Gingold and J. J. Monaghan, Mon. Not. R. Asron. Soc. **181** (1977), 375.
3) D. Wood, Mon. Not. R. Astron. Soc. **194** (1981), 201.
4) S. M. Miyama, C. Hayashi and S. Narita, Astrophys. J. **279** (1984), 621.
5) M. Sekiya, S. M. Miyama and C. Hayashi, Earth Moon Planets **39** (1987), 1.
   S. M. Miyama, S. Narita and C. Hayashi, Prog. Theor. Phys. **78** (1987), 1273.
   S. Watanabe and S. M. Miyama, Astrophys. J. **391** (1992), 318.
   S. M. Miyama, Publ. Astron. Soc. Jpn. **44** (1992), 193.
6) J. J. Monaghan, Annu. Rev. Astron. Astrophys. **30** (1992), 543.
7) R. F. Stellingwerf, Lecture Note in Physics **395** (1991), 239.
8) L. D. Libersky and A. G. Petschek, Lecture Note in Physics **395** (1991), 248.
9) L. D. Libersky, A. G. Petschek, T. C. Carney, J. R. Hipp and F. A. Allahdadi, J. Comput. Phys. **109** (1993), 67.
10) A. G. Petschek and L. D. Libersky, J. Comput. Phys. **109** (1993), 76.
11) W. Benz, W. L. Slattery and A. G. W. Cameron, Icarus **71** (1987), 30.
12) A. G. W. Cameron and W. Benz, Icarus **92** (1991), 204.
13) S. Inutsuka, Doctor Thesis and to be submitted to J. Comput. Phys. 1994.
14) G. E. Eggum, F. V. Coroniti and J. I. Katz, Astrophys. J. **323** (1987), 634.
    W. Kley and G. Hensler, Astron. Astrophys. **172** (1987), 124.
    W. Kley, Astron. Astrophys. **247** (1991), 95.
    W. Kley and D. N. C. Lin, Astrophys. J. **397** (1992), 600.
15) H. Takeda, T. Matsuda, K. Sawada and C. Hayashi, Prog. Theor. Phys. **74** (1985), 272.
16) H. Takeda, Prog. Theor. Phys. Suppl. No. 96 (1988), 196.
17) G. Shaviv and E. E. Salpeter, Astron. Astrophys. **110** (1982), 300.
18) L. Brookshaw, Proc. ASA **6** (2) (1985), 207.
19) S. M. Miyama, Soryushiron Kenkyu (Kyoto) **82** (1990), A27.
20) J. J. Monaghan, Comput. Phys. Comm. **48** (1988), 89.

21) S. Taneda, J. Phys. Soc. Jpn. **11** (1956), 302.
M. Coutanceau and R. Bouard, J. Fluid Mech. **79** (1977), 231.
22) H. Takami and H. B. Keller, Phys. Fluids Suppl. **II** (1969), 51.
S. C. R. Dennis and Gau-Zu Chang, J. Fluid Mech. **42** (1970), 471.
B. Fornberg, J. Fluid Mech. **98** (1980), 819.
V. A. Patel, J. Comput, Phys. **71** (1987), 65.
23) R. L. Underwood, J. Fluid Mech. **37** (1969), 95.
24) F. Nieuwstadt and H. B. Keller, Comput. Fluids. **1** (1973), 59.
H. Jafroudi and H. T. Yang, J. Comput. Phys. **49** (1983), 181.
25) Y. Shida and K. Kuwahara, AIAA Paper (1985), 85-1692.
26) S. Osher and S. Chakravarthy, J. Comput. Phys. **50** (1983), 447.
K. Sawada, E. Shima, T. Matsuda and T. Inaguchi, in *Computational Gas Dynamics of Accretion Flows*, ed. T. Matsuda (Report for Grant-in-Aid for Scientific Research) (1986), p. 109.
27) J. C. Latanzio, J. J. Monaghan, H. Porgracic and M. P. Schwarz, Mon. Not. R. Astron. Soc. **215** (1985), 125.